Indonesian Journal of Science & Technology

Journal homepage: http://ejournal.upi.edu/index.php/ijost/

A New Multicarrier Sinusoidal Pulse Width Modulation (SPWM) Strategy based on Rooted Tree Optimization (RTO) Algorithm for Reducing Total Harmonic Distortion (THD) of Switched-Capacitor Nine-level Inverter in Grid-connected PV systems

H.Aboub[1], R.Mechouma[1], B.Azoui[1], C. Labiod[2], A. Khechekhouche[3,]*

[1] Department of Electrical Engineering, Laboratory LEB, University of Batna 2, Batna, Algeria
[2] Laboratory of Energy Systems Modeling: LMSE, University of Biskra, BP 145, Biskra 07000, Algeria
[3] Development Renewable Energy Unit in Arid Zones (UDERZA), University of El Oued, Algeria
Correspondence: E-mail: abder03@hotmail.com

ABSTRACT

This paper proposed a new strategy of sinusoidal pulse width modulation (SPWM) technique to control three-phase nine-level switched-capacitor inverter (9LSCI) in grid-connected PV systems. The main advantage of this inverter is high voltage gain, achieved by switching the capacitors in series and parallel to boost up the output voltage using low voltage input. To improve the quality of solar energy for injection into the electrical grid, a rooted tree optimization (RTO) algorithm is used to get optimum values of initial angles of multi carriers SPWM technique, giving the lowest possible values of the total harmonic distortion (THD). The design also can maximize the efficiency of the multi-level inverter by minimizing its size using fewer components and a single DC source and reducing the rate of THD. The higher effectiveness and accuracy of the suggested RTO-SPWM technique was tested and verified in comparison to existing classical SPWM technique from the performance of PV-grid systems that it can effectively reduce the total harmonic distortion to 0.16 %.

ARTICLE INFO

Article History:
Submitted/Received 03 Sep 2021
First revised 08 Oct 2021
Accepted 15 Dec 2021
First available online 20 Dec 2021
Publication date 01 Apr 2022

Keyword:
Fuzzy logic controller,
Grid-connected PV system,
Rooted tree optimization,
Multi Carriers SPWM technique,
Total harmonic distortion,
Switched-capacitor inverter.

1. INTRODUCTION

Photovoltaic grid-connected systems have become highly important nowadays because they offer good solutions to overcome emissions by reducing the use of f ossil fuels. Especially in high PV power applications, multi-level inverters (MLI) have been recognized as a major alternative to the classical two-level H-bridge inverter, to produce higher output voltage with lower switching frequency and lower total harmonic distortion**.** In literature, conventional MLI are classified into three categories: Neutral Point Clamped (NPC), Flying Capacitor (FC), and Cascaded H-Bridge Inverter. Among them, NPC and FC give a common DC-link, which is a rigorous requirement for many applications (Youssef *et al.*, 2019)**.** However, an excessive number of clamping diodes and FC increases the primary cost and maintenance surcharges and reduces the accuracy of the inverter. Furthermore, the maximum output voltage is half of the input DC voltage in these topologies. On the other hand, the cascaded H-bridge MLI topology requires a separated DC source for each H-bridge and a separate DC source for each phase**.** Otherwise, all these MLI's topologies need more components and high input voltage and suffer from capacitor self-voltage balancing problems or high-voltage stress on switches when injecting the PV energy in the grid. Consequently, it is appropriate to improve boost the DC/DC converter with a higher conversion ratio or create a particular topology for MLI that has a less number of components and uses a lower DC voltage. Many researchers proposed MLI with reduced components that have been reported in the literature. Among these topologies, there is the switched capacitor converter (SCC). It uses this structure in two main ways:

Either as a step-up DC converter or as a multi-level AC waveform when it is connected with a classical H-bridge inverter. It has fewer components and uses a lower DC voltage supply (Sandeep & Yaragatti, 2017). Many types of research are conducted on the new topology of switched-capacitor inverters, a seven-level switched-capacitor inverter using sinusoidal pulse width modulation (SPWM) technique was presented (Teja *et al.*, 2017). Also, a comparative study of seven-level switched-capacitor inverters was proposed by using the same technique for a very weak input voltage**.** Besides, to validate the performance of a single-phase nine-level switched-capacitor converter in a PV system, simulations and experimental tests are achieved with a simple harmonic elimination technique (Nouaiti *et al.*, 2017)**.** The same authors realize a stand-alone PV system application using a single-phase five-level switched-capacitor inverter (Nouaiti *et al.*, 2018). Also, a five-level switched-capacitor inverter based on grid-connected PV Systems with reduced components was realized. Furthermore, a switched-capacitor inverter for PV power systems was proposed for submersible pumps in agricultural applications using the artificial neural network. In addition, Qi *et al.*, (2021) was proposed sliding mode controller to control switched-capacitor-based high DC for photovoltaic applications. All these researches assured that the switched capacitor topology of inverters create a greater output voltage compared to the input voltage by correctly selecting the switching control capacitors in series and parallel.

Moreover, many scientists developed various techniques and methods to control the switching for MLI intending to reduce the total harmonic distortion (THD)**,** such as the space vector pulse width modulation (SVPWM), selected harmonic elimination pulse with modulation (SHEPWM), and SPWM (Meraj *et al.*, 2020). This last technique is the most used to control MLI due to its simplicity and ease of implementation. It is based on the

DOI: http://doi.org/10.17509/ijost.v7i1
p- ISSN 2528-1410 e- ISSN 2527-8045

comparison of a sinusoidal reference signal with carrier signals having the same frequency, which are usually selected as triangular pulses. In each carrier waveform, there are different techniques such as Phase Disposition PD, inverted phase disposition IPD, phase opposition disposition POD, and alternative phase opposition disposition APOD (Tariq *et al.*, 2018). Regarding the PD procedure, m-1 carrier waveforms are demanded for m-level phase waveforms, which are compared with a sine wave. For(m-1/2) carrier waves, the upper zero references are in phase and the rest of carrier waves below the reference are also in phase. In the POD method, the (m-1/2) carrier waves below the reference are in phase but the phase-shift is 180° (π rad) from those above zeros. However, in the APOD method, m-1 carrier waveforms are phase displaced by 180 degrees alternately. To improve the values of THD in MLI, the technique suggested in this manuscript is based on the idea of varying the initial angles of each carrier wave of the SPWM technique instead of fixing them, these angles are calculated using an optimal calculation system.

In the literature, different techniques for improving inverter performance have been suggested to find the lowest values of THD such as; Analysis of THD for seven-level asymmetrical cascaded H-Bridge MLI using the LSCPWM technique (Singh, 2015). An optimized modified PWM technique based on differential evolution on NPC Inverter. In modified hybrid pulse width modulation strategy was modeled for reduced THD in seven level inverters. Swarm Optimization (SO) algorithm is used to minimize harmonics in MLI based on the SHEPWM technique which is a complex optimization problem relevant to a nonlinear transcendental equation (Gopal *et al.*, 2019). In addition, the authors were using a genetic algorithm to solve the optimization of the SHEPWM technique on seven-level cascaded MLI based on natural selection to reduce THD (Mali & Patil, 2018). Also, a firefly-assisted genetic algorithm for SHEPWM was applied in PV interfacing to reduce THD in seven-level inverters in Sen *et al.* (2019). In recent years, novel strategies to solve the issue problem of optimization via an easy-to-implement is nature-inspired Rooted Tree Optimization (RTO) algorithm based upon the imitation of the natural behavior of tree roots searching for a place that has the most water (Labbi *et al*, 2016). The wetness degree (WD) of the root head determines the roots' orientation, they move at random in search of water, but when one or more roots detect moisture, they signal to others to update their way to be closer to the source of water, i.e. the best solution (Benamor *et al.*, 2019; Sannigrahi *et al.*, 2019).

The main contribution of this article is the use of the new strategy of the multi-carrier SPWM technique to control the switched capacitor multi-level inverter (9LSCI) proposes that the initial angles of the carriers are variable and that their optimized values be calculated by an RTO algorithm to obtain less THD to improve the efficiency and quality of the solar energy fed into the grid.

2. METHOD

Table 1 shows the acronym used in this study. Our new idea proposes a new strategy of SPWM technique to control three phases nine-level switched-capacitor inverter (9LSCI) in grid-connected PV systems which are based on the variation of the initial angles of each carrier wave of SPWM technique unlike all the other techniques discussed so far, these angles are calculated using an optimal calculation system.

DOI: http://doi.org/10.17509/ijost.v7i1
p- ISSN 2528-1410 e- ISSN 2527-8045

Table 1. The nomenclature used in this study.

Acronyms	Meaning
MLI	Multi-Level Inverter
SCI	Switched-capacitor inverter
9LSCI	Nine-level switched-capacitor inverter
SPWM	Sinus Pulse With Modulation
FFT	Fast Fourier Transformer
THD	Total Harmonic Distortion
PD	Phase Disposition
IPD	Inverted Phase Disposition
POD	Phase Opposition Disposition
APOD	Alternative Phase Opposition Disposition
PIC	Proportional Integral Controller
FLC	Fuzzy Logic Controller
RTO	Rooted Tree Optimization
MPP	Maximum Power Point Tracking
PV	Photovoltaic
WD	Witness Degree
Symbols	
I_{pv}	Photovoltaic current (A)
I_{sa}	diode inverse saturation current (A)
I_{ph}	photo current
V_{th}	thermal voltage (V)
V_{oc}	PV open circuit voltage (V)
I_{CC}	PV short-circuit current (A)
I_{op}	optimal PV current (A)
V_{op}	Optimal PV voltage (V)
D_{pv}	Boost duty cycle
V, V_{ref}	actual and reference voltage (V)
I, I_r	actual and reference current (A)
E, E_r	actual and reference insolation (W/m^2)
I_{dcref}	Reference DC bus current(A)
$V_{DC\text{-}BUS}$	DC bus voltage (V)
R_s	Serie resistance
R_{sh}	Shunt resistance
I_d, I_{dref}	actual and reference direct grid current (A)
I_q,I_{qref}	actual and reference quadratic grid current (A)
L_f	Filter inductance (h)
C_f	Filter capacitance (F)
R_r	Rate of random roots
R_c	Rate of continued roots
R_n	Rate of nearest roots

A rooted tree optimization RTO algorithm is proposed to search for optimum values of initial angles which gives the lowest possible values of the total harmonic distortion THD. This algorithm is inspired by nature that was recently adopted which simulates the tired technique for roots trees in search of water. As a majority of search methods, it begins to create an initial random generation and calculate the witness degree at each root, then arrange these roots in ascending order according to the witness degree. The next

DOI: http://doi.org/10.17509/ijost.v7i1
p- ISSN 2528-1410 e- ISSN 2527-8045

generation is created depending on the previous generation, where the roots with a high degree of witness are preserved, and the roots with a very weak are canceled and replaced with the highest ones depending on the Special mathematical equations and in each generation, we determine the optimal solution that gives the lowest value for THD.

To improve the quality of solar energy for injection into the electrical grid by using fewer components, a 9LSCI can be used which is achieved by switching the capacitors in series and in parallel to boost up the output voltage by using low voltage input with appropriate switching control. To produce various signals of switches of this inverter, the RTO- SPWM proposed technique is used to reduce the values of THD of grid current. The higher effectiveness and accuracy of the suggested RTO-SPWM technique is tested and verified in comparison to existing classical SPWM technique from the performance of PV-grid systems by Matlab computer programming that it can effectively reduce the total harmonic distortion to 0.16 %. with better dynamic performances. The following points explain the steps of our method:

(i) The system design and modeling process studied as shown in **Figure 1** is including a detailed description of the proposed model of 9LSCI.

(ii) The fuzzy logic controller FLC is applied to control the MPPT of the PV generator, to regulate the voltage V dc-Bus which represents the input of 9LSCI. It should be noted that the control of the gate current is carried out by FLC.

(iii) The process used to manipulate the RTO algorithm of the SPWM control strategy is presented with discrete variables and defines the design parameters: the constraints and the adequacy of the optimization problems are explained by the flowchart.

2.1. Design and Modeling of a Grid-Connected PV System Based on 9LSCI

The architecture of the proposed grid-connected PV system is shown in **Figure 1**, which consists of a photovoltaic generator for each phase of 5 kW composed of five strings of 14 modules each. A DC/DC boost converter is used to extract the maximum energy from the PV array by using the FLC and a 9LSCI is used to inject this PV power into the grid with an LC filter. To control the switching states of 9LSCI, an RTO algorithm is proposed to search for optimum initial angles of multi carriers SPWM strategy to ameliorate the THD of the current output injected into the grid.

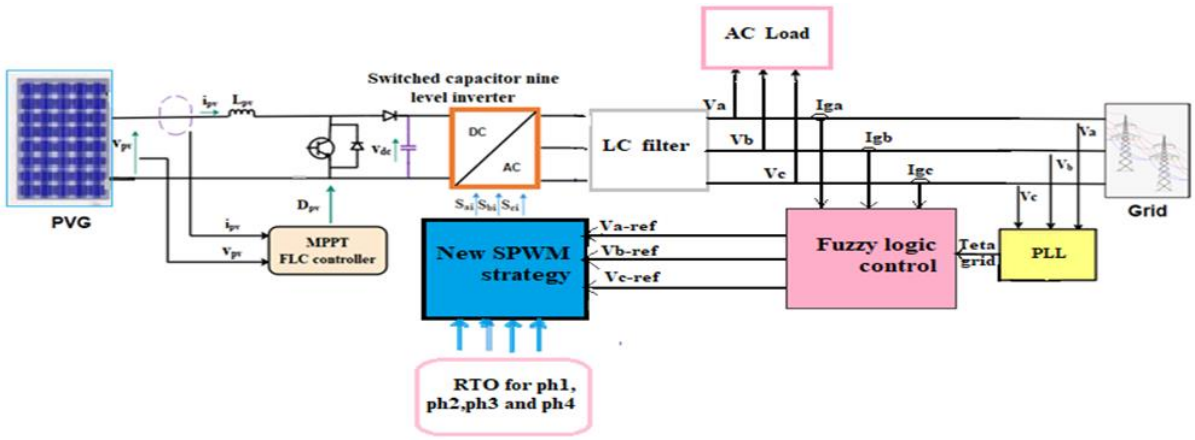

Figure 1. The architecture of a grid-connected PV system with three phases 9LSCI.

DOI: http://doi.org/10.17509/ijost.v7i1
p- ISSN 2528-1410 e- ISSN 2527-8045

2.2. Model of Proposed 9LSCI

Figure 2 indicates the structure of the suggested 9LSCI, which is accomplished by cascading two circuits, an SCC and an inverter of two levels full-bridge (Nouaiti *et al.*, 2017; Tariq *et al.*, 2018). This must first be converted to a high DC voltage before being converted to AC Current. This topology can be used to get any number of levels with the help of series-parallel conversion operations. It consists of some Switched-Capacitor (SC) cells, as each SC cell consists of one capacitor and two switches. Several output voltage levels can be obtained from one input voltage (Teja *et al.*, 2017).

The control circuit of the 9LSCI connected with the grid is depicted in **Figure 3**. It is based on the use of Fuzzy Logic control in a closed-loop (Maamir *et al.*, 2020; Tiar *et al.*, 2017). It consists of three FLC regulators: The first regulator is used to regulate the DC Bus voltage of the inverter that minimizes the error between VDC-Ref and the sensed voltage. The regulator's output has the reference of the direct grid current. The second FLC works on minimizing the error between the sensed current Id and the generated reference current Id-Ref from the first FLC. The third FLC regulator is used to adjust the quadratic grid current to the value of zero.

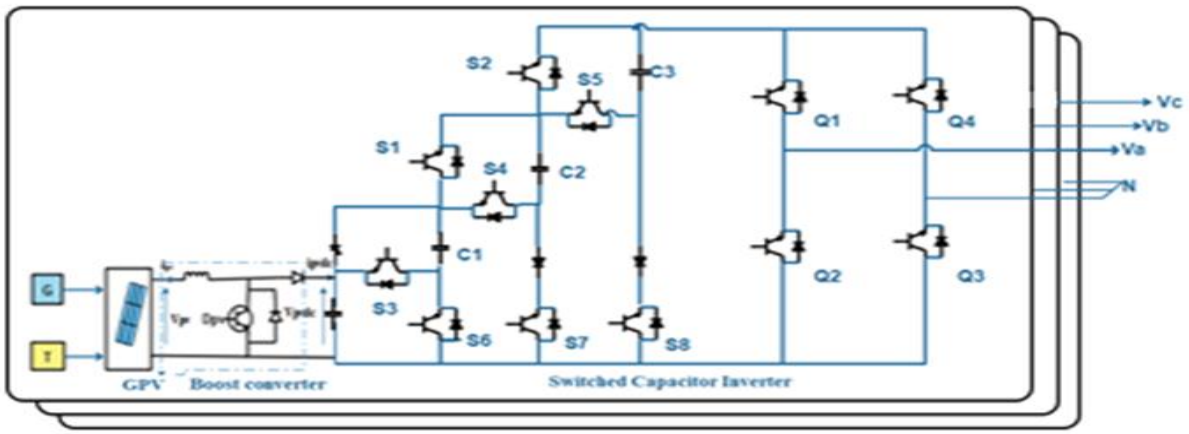

Figure 2. Topology of a single phase of 9LSCI.

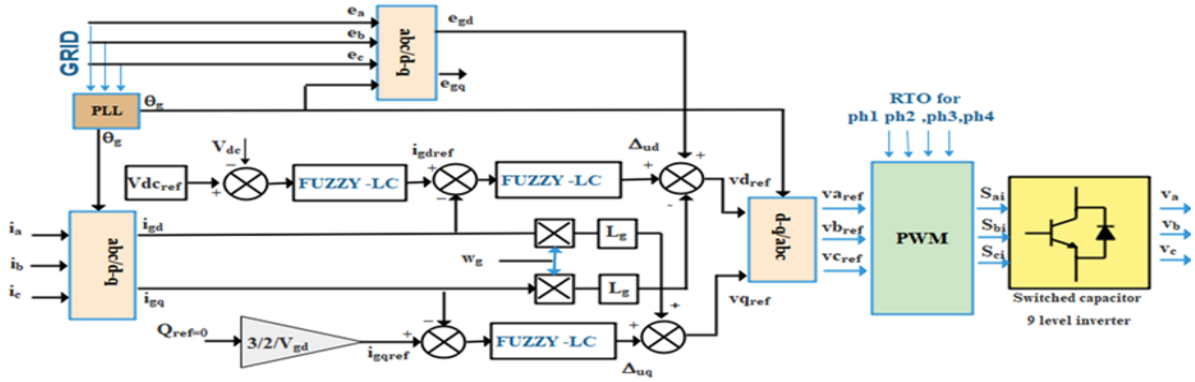

Figure 3. Block diagram of fuzzy logic control of grid current.

DOI: http://doi.org/10.17509/ijost.v7i1
p- ISSN 2528-1410 e- ISSN 2527-8045

2.3. Process of RTO algorithm applied on SPWM technique

To determine the minimum THD value of grid current, the optimal initial angles *Ph1, Ph2, Ph3* and *Ph4* in the proposed multi carriers SPWM technique is calculated by using rooted tree optimization technique RTO to control the 9LSCI of the grid-tied PV system.

In the process of the RTO, the algorithm begins by randomly generating an initial population consisting of *P* roots within the search space.

The solutions of each population are first reordered as a whole WD (*k*) to find the best solution in the next step. The roots are sorted in a descending way according to the values of *WD*. Therefore, the best solution is the smallest THD value of each generation. Thus the scenario of the RTO algorithm is based on the choice of the best solutions for the current population as individuals in the next generation. Further clarification concerning the RTO algorithm applied to search for optimum angles of multi carriers SPWM strategy to control 9LSCI is brought up in the flowchart as shown in **Figure 4**.

3. RESULTS AND DISCUSSION

The various simulations were performed under the package MATLAB / Simulink environment. To test the performance and the effectiveness of the proposed RTO algorithm to control the switching of 9LSCI in a PV grid-connected system, the load power, and the solar irradiance are varied in step over a time span of 2 s as shown in **Figures 5** and **6**, the solar irradiance takes the value of 500 W/m^2 between 0 and 0.8 s, 700 W/m^2 between 0.8 and 1 s, increases to 800 W/m^2 at t=1s, and takes its higher value (1000 W/m^2) between 1.5 and 2 s; A FLC used on the side of PV generator to extract the maximum power point is rendering the response of the MPPT faster to block any unforeseen and quick variation of climatic conditions.

The parameters of the proposed system are selected in **Table 2** to meet the requirements of the grid and solar energy. Our control system uses also an FLC to regulate V_{dc_Bus} that represents the input of the 9LSCI, as depicted in **Figure 3**, where this latter needs four carriers PWM signals for its switching control whose initial angles are calculated in this study by the rooted tree optimization algorithm.

Table 3 presents the parameters of the RTO algorithm, while **Table 4** is the detail of the optimal results of this algorithm. For the choice of the parameters of the RTO-SPWM, in particular the number of iterations, it was set as 20 (i.e. we started with 5 then 10 then 15, and finally 20, which gave satisfactory simulation results).

Figures 7 and **8** show the convergence curves of the fitness function and the wetness degree of the RTO algorithm, respectively. Therefore, we noted the stability and convergence after iteration number 20.

Figure 9 presents the evolution of the best parameters *Ph1, Ph2 Ph3 & Ph4* according to the number of iterations, while **Figure 10** shows the image of the carrier signals of the best angles that are calculated by the RTO algorithm. The results of simulations of the overall system are shown.

DOI: http://doi.org/10.17509/ijost.v7i1
p- ISSN 2528-1410 e- ISSN 2527-8045

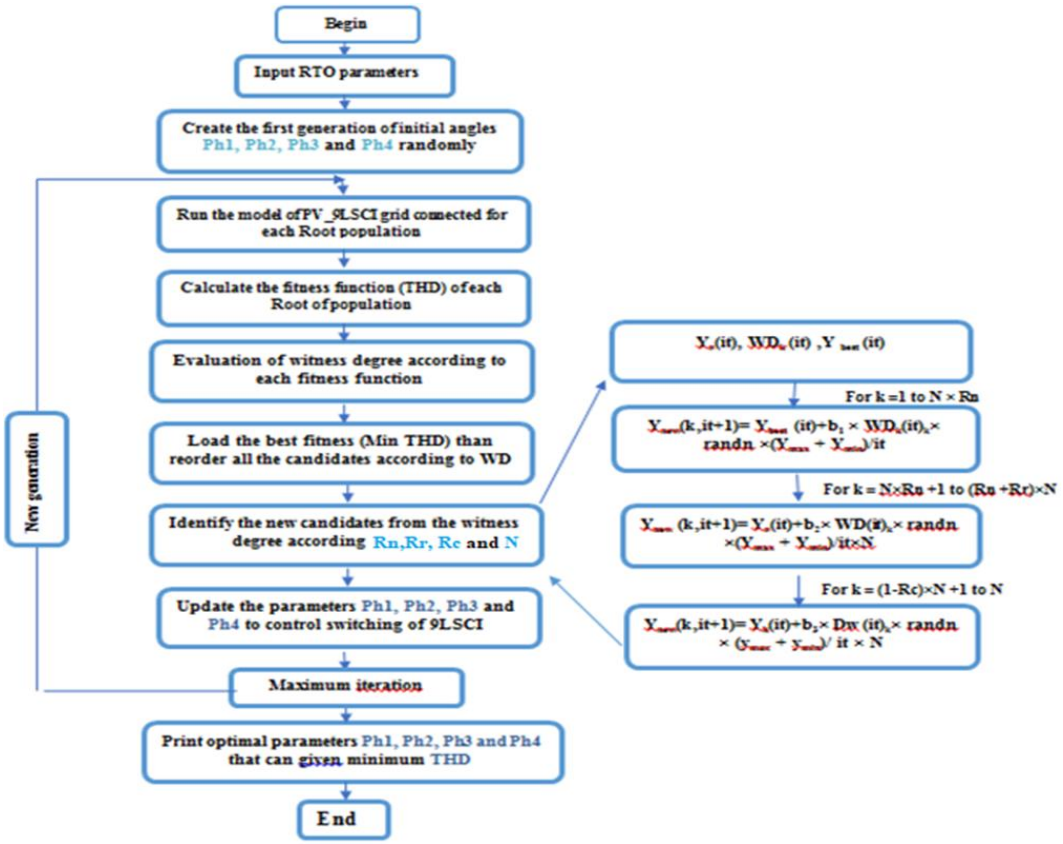

Figure 4. Flowchart of the RTO algorithm. *N* is the number of candidates in the population. *It* is the number of iteration. *K* is the candidate number. *Dim* is the Dimension of the RTO algorithm. $Y_r(it)$ is the random candidate for the actual iteration. $Y_{best}(it)$ is the best candidate for the actual iteration. $Y_k(it)$ is the previous candidate for the actual iteration. Y_{min}, Y_{max} is The minimum and maximum of the value of a candidate, respectively. R_c based on roots continuity that is can be continued in the next generation. R_n is the presents the coefficient of the nearest root to water that can create a new generation with the death of distant roots. R_r depends on the random root. Knowing that the variables (R_r, R_c, R_n) must be chosen to verify the condition is the $R_n+R_c+R_r=100\%$.

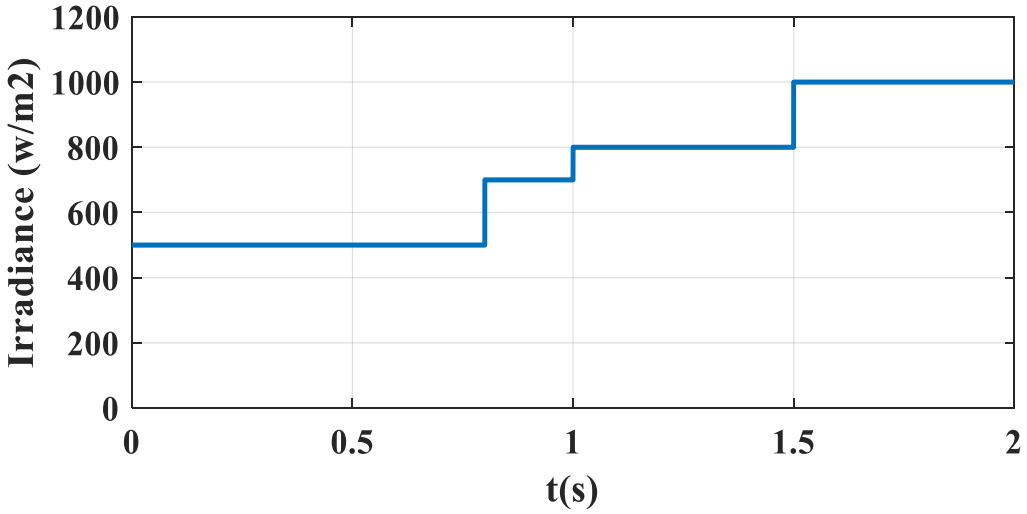

Figure 5. Variation of irradiation levels

DOI: http://doi.org/10.17509/ijost.v7i1
p- ISSN 2528-1410 e- ISSN 2527-8045

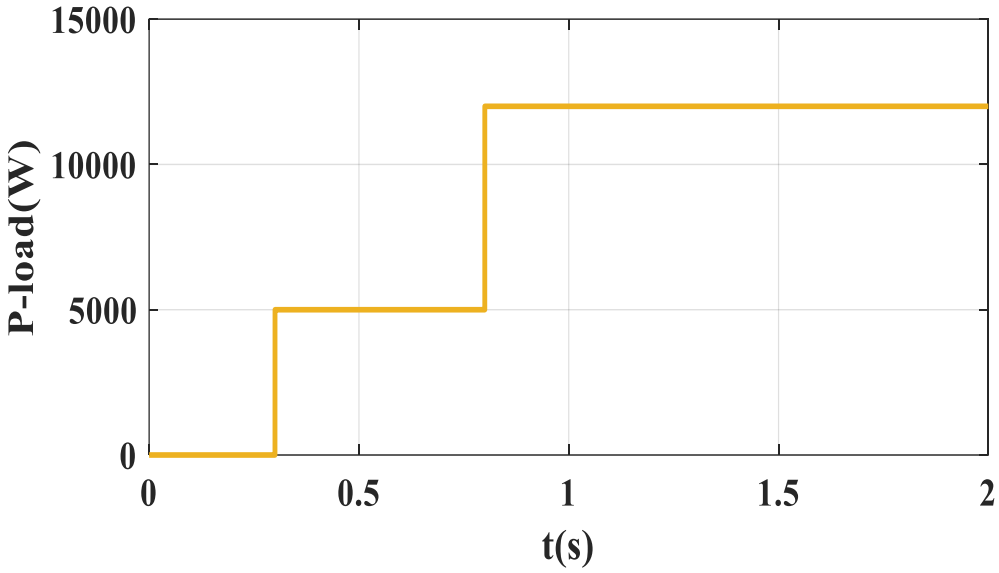

Figure 6. The demand for load power.

Table 2. Parameters of the proposed system.

Sources	Parameters	Values
PV generator	Iop	4.34.A
	Icc	4.67 A
	Voc	21.6 V
	Vop	17.3 V
	Pop	75 W
9LSCI	C_1, C_2, C_3	1000 µF
	$V_{DC\ input}$	100 V
	$V_{DC\ BUS}$	400 V
LC FILTER	L_f	0.02 h
	R_f	0.2 Ohm
	C_f	0.2 µF
Electrical grid	V-RMS	311 V

Table 3. Parameters of the RTO algorithm.

Parameters	Values
RTO Size	20.0
Max iteration	50.0
DIM	4.0
b1	0.2
b2	2.0
b3	1.2
R_n	0.3
R_n	0.3
R_n	0.4
Ph1	[0, 2π]rd
Ph2	[0, 2π]rd
Ph3	[0, 2π]rd
Ph4	[0, 2π]rd

DOI: http://doi.org/10.17509/ijost.v7i1
p- ISSN 2528-1410 e- ISSN 2527-8045

Table 4. The fitness value of each optimal root.

Iteration N°	Optimal Angel (*rd*)	Fitness Function THD %
1	Ph1= 4.2646	0.34
	Ph2=4.7610	
	Ph3=4.6692	
	Ph4=2.4644	
5	Ph1=5.6334	0.28
	Ph2=3.5340	
	Ph3=4.9457	
	Ph4=1.1826	
10	Ph1=5.6337	0.26
	Ph2=3.5359	
	Ph3=4.6467	
	Ph4=1.1815	
50	Ph1=5.6273	0.16
	Ph2=3.5350	
	Ph3=4.9503	
	Ph4=1.1712	

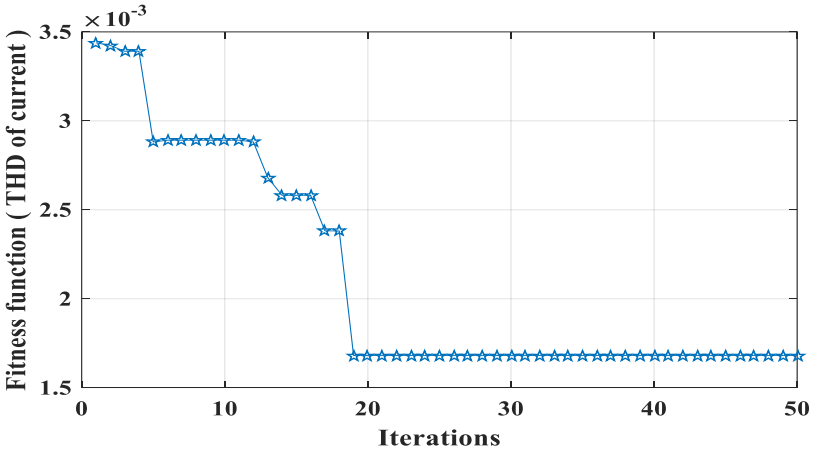

Figure 7. Convergence curves of RTO for the fitness function.

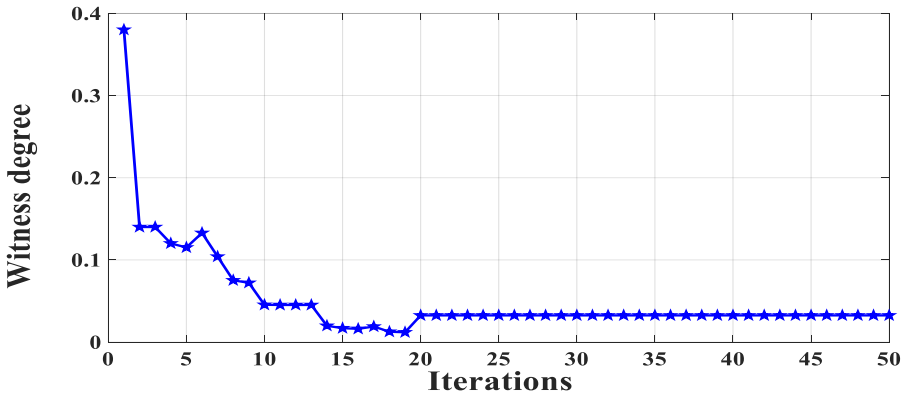

Figure 8. Wetness Degree of RTO.

DOI: http://doi.org/10.17509/ijost.v7i1
p- ISSN 2528-1410 e- ISSN 2527-8045

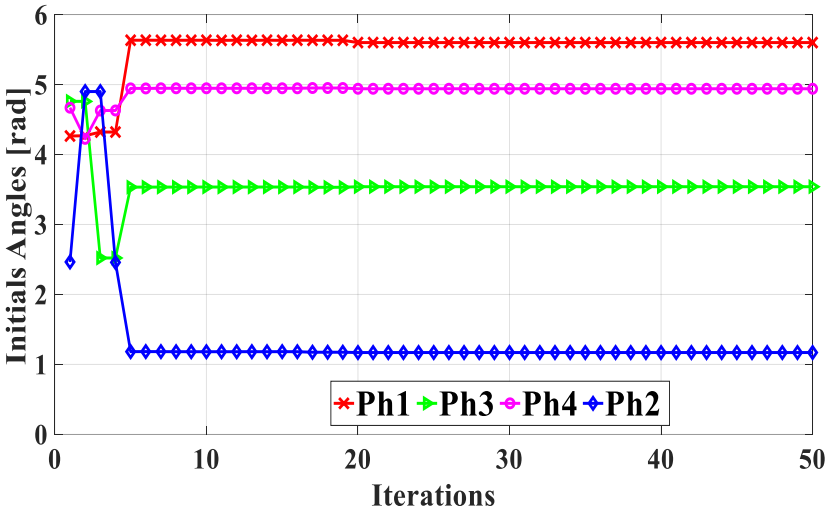

Figure 9. Optimal initial angles of each generation.

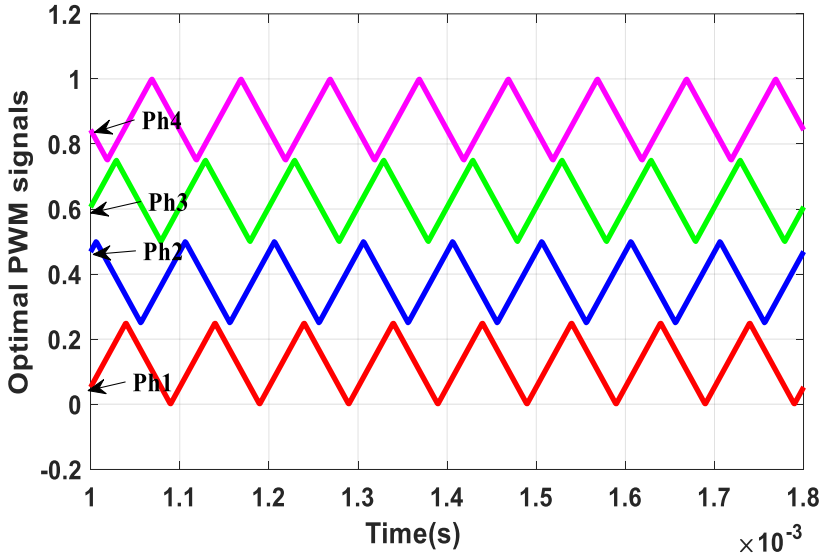

Figure 10. Carriers signals according to optimal angles for RTO.

Figure 11 shows the output power of the PV generator, the load power, and the grid power. It can be remarked in **Figure 12.** that the introduced FLC gives the fast dynamic response of the DC-link voltage compared to the PIC controller, which demonstrates the robustness of FLC with high rapidity.

Figures 13 and **14** show the direct and quadratic grid current respectively. **Figure 15** presents the grid current of phase (a), while **Figure 16** displays three phases of electrical grid current.

Figure 17(a) shows the voltage and current grid in the time interval from 0.1 to 0.2 is it can be observed that the current grid is in phase with the voltage waveform. However in the time between [0.9 and 1], the power grid is injected into the load, so the current and the voltage of the electrical grid are in opposition of phase as shown in **Figure 17 (b)**. **Figure 18** shows the FFT result of the output voltage waveform of 9LSCI and its THD according to the control used. **Figure 19** displays the spectrum analysis of the current grid, which has a sinusoidal waveform.

DOI: http://doi.org/10.17509/ijost.v7i1
p- ISSN 2528-1410 e- ISSN 2527-8045

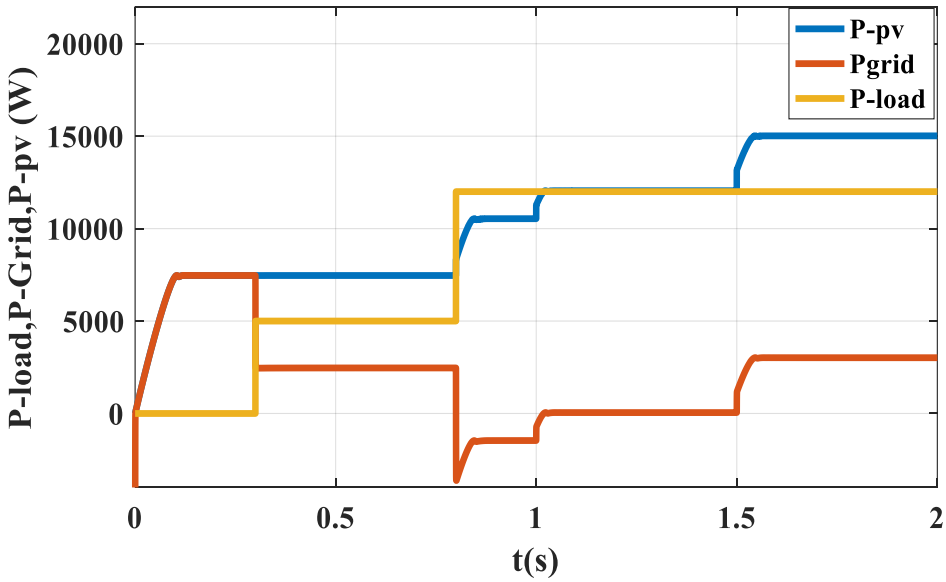

Figure 11. PV, Load, and grid power

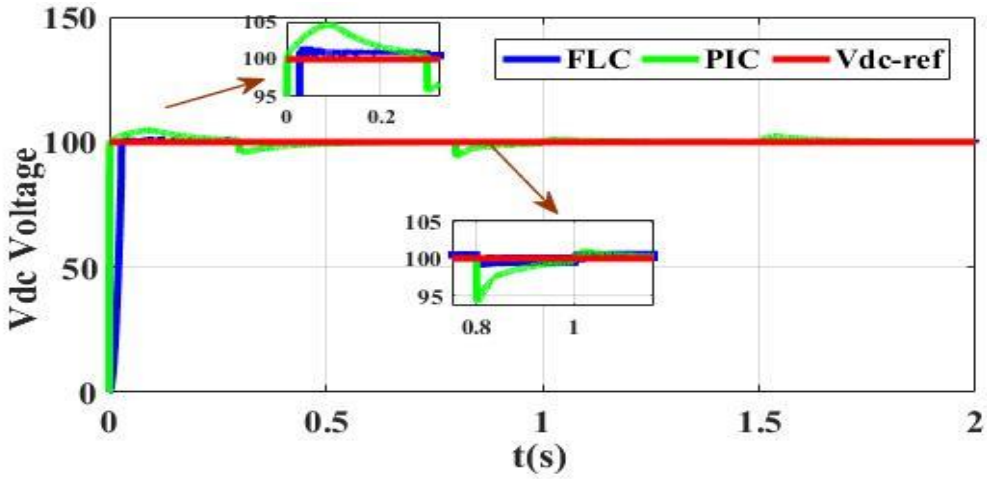

Figure 12. Input voltage of 9LSCI.

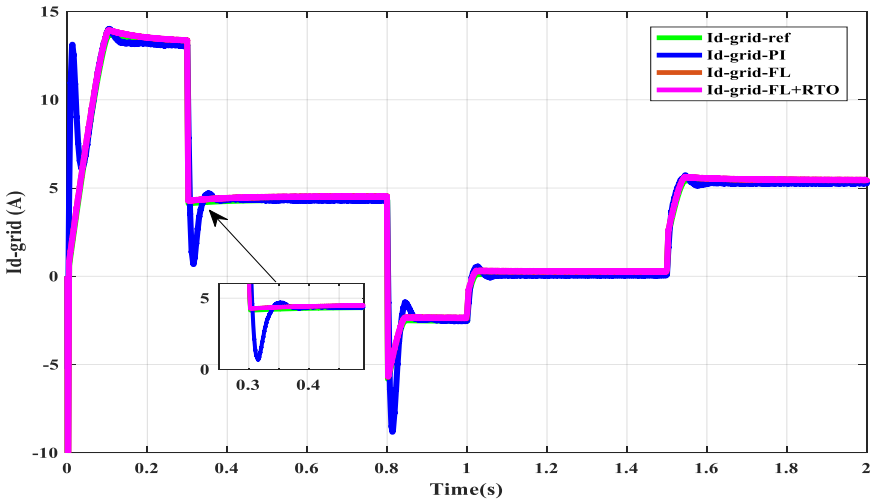

Figure 13. Direct grid current.

DOI: http://doi.org/10.17509/ijost.v7i1
p- ISSN 2528-1410 e- ISSN 2527-8045

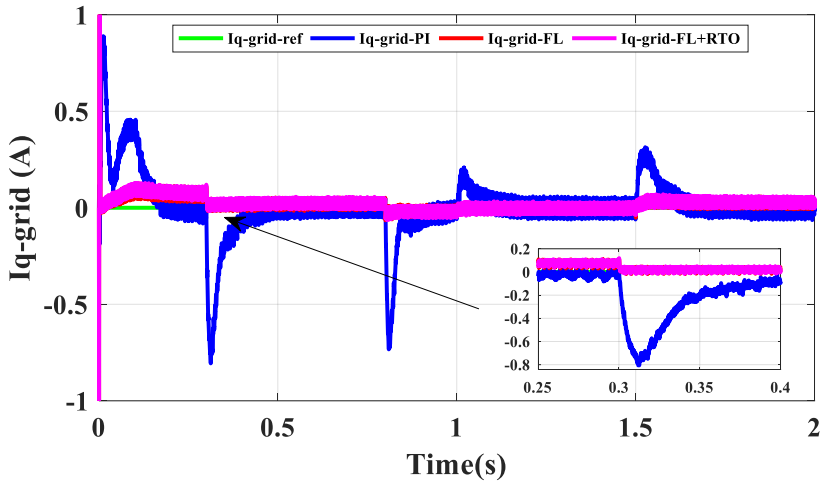

Figure 14. Quadratic grid current.

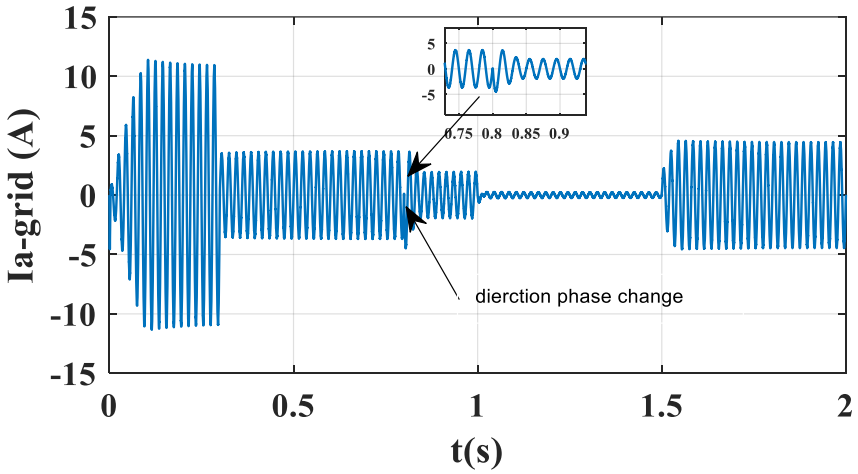

Figure 15. Grid current of phase 'a'.

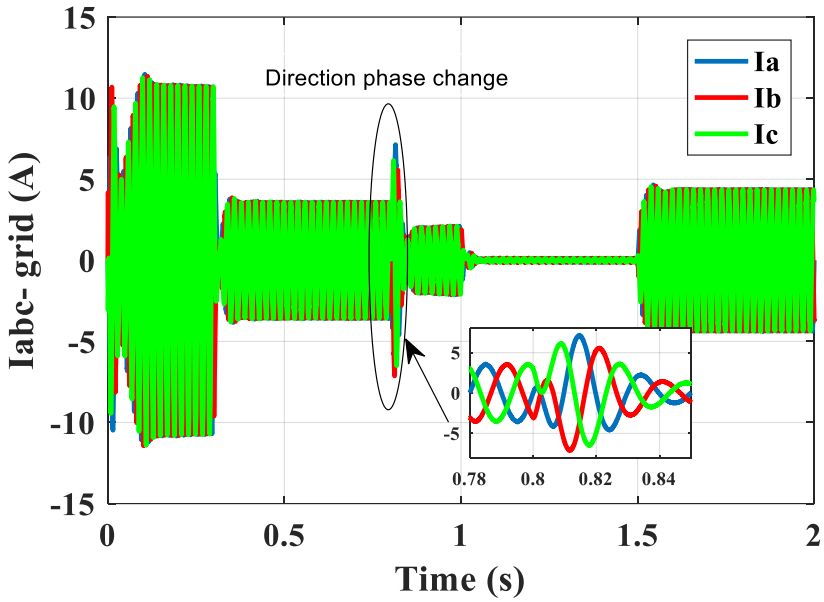

Figure 16. Three-phase grid current.

DOI: http://doi.org/10.17509/ijost.v7i1
p- ISSN 2528-1410 e- ISSN 2527-8045

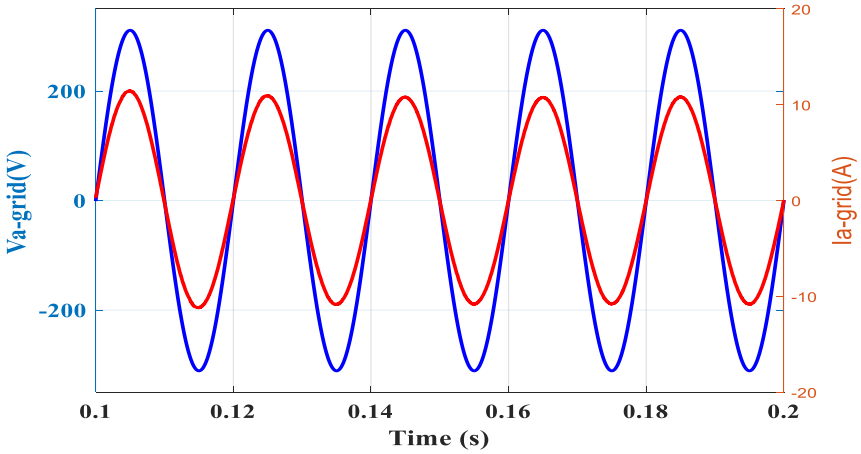

(a)

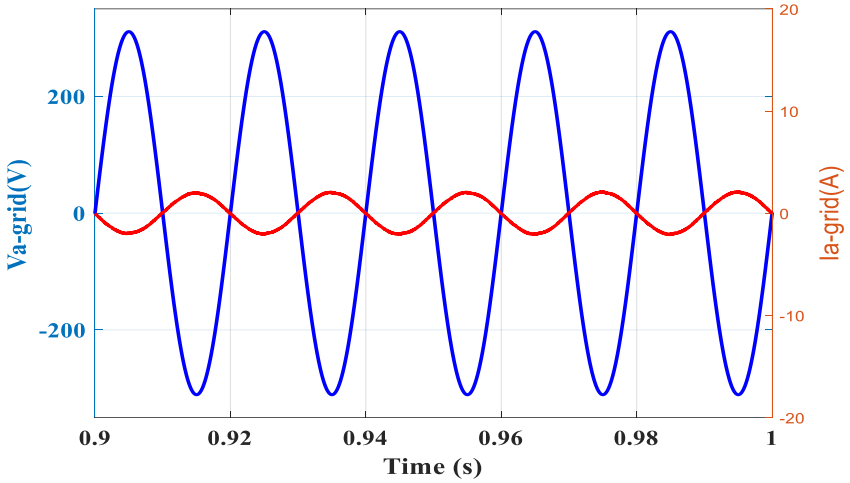

(b)

Figure 17. Voltage and current grid of phase a. Figures **(a)** is the PV power is injected into the grid, and Figure (**b)** grid power is injected in the load

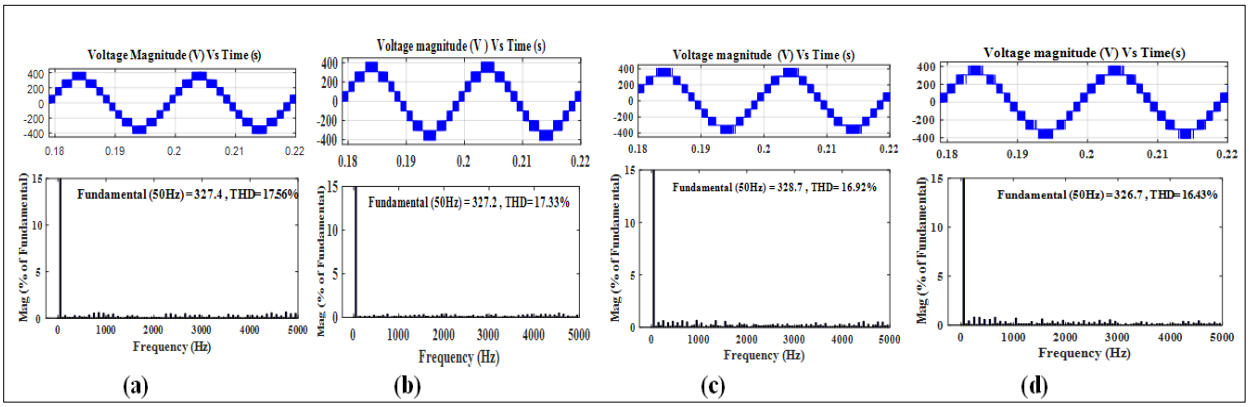

(a) (b) (c) (d)

Figure 18. Harmonic spectra of the output voltage of SC9LI with is the (a) PI-PD-SPWM, (b) FL-PD-SPWM (c) PI-RTO-SPWM, and (d) FL-RTO-SPWM.

DOI: http://doi.org/10.17509/ijost.v7i1
p- ISSN 2528-1410 e- ISSN 2527-8045

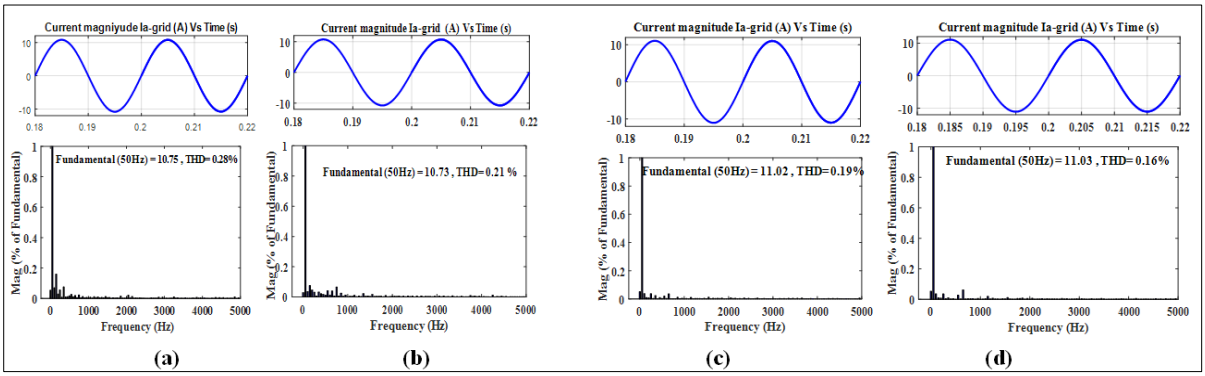

Figure 19. Harmonic spectra of the current grid of SC9LI with is the (a) PI-PD-SPWM, (b) FL-PD-SPWM (c) PI-RTO-SPWM, and (d) FL-RTO-SPWM.

Based on **Table 5**, a comparative analysis of different controllers has been carried out to check the performances of the multi carriers SPWM based on the RTO algorithm.

Finally, to check the accuracy and feasibility of the RTO-SPWM technique to obtain the optimal THD, the simulation results are compared with the other strategy of switching control in the literature. The comparison is depicted in **Table 6**.

Table 5. Comparison to multi carriers SPWM technique and different controller types.

Multi carriers SPWM	Parameters of initials angles of PWM signals(rad)				Fitness Function THD
	Ph1	Ph2	Ph3	Ph4	
PI-PD-PWM					0.28
FL-PD-PWM	0	0	0	0	0.21
PI-RTO-PWM	5.6273	3.5350	4.9503	1.1712	0.19
FL-RTO-PWM					0.16

Table 6. Comparison according to THD of each SPWM technique and type of MLI.

References	Type of MLI	Type of PWM	THD (%)	
			Current (Ia)	Voltage (Va)
(Meraj *et al*., 2020)	7L- CI	PODPS-PWM	2.20	31.02
		SPWM-3 cycle	2.18	32.37
(Tariq *et al*., 2018)	7L- PUCI	Traingle PD-SPWM	4.90	18.34
		Sawtooth PD-SPWM	4.54	17.99
(Marmouh *et al*, 2018)	9L-CI	OCC-SVMPWM	-	17.37
Our study	9L-SCI	PD-SPWM	0.21	17.33
		RTO-PD-SPWM	0.16	16.43

DOI: http://doi.org/10.17509/ijost.v7i1
p- ISSN 2528-1410 e- ISSN 2527-8045

3.1. Discussion

Figures 7 and **8** show that the RTO algorithm has better performance, in terms of rapidity, accuracy, and stability, and it works well with complex systems as the classical techniques. During the time interval [0 and 0.3s] is the MPPT algorithm is allowed, the PV array power is injected into the grid, where the direct grid current tracks its reference perfectly (**Figure 13**), then the phase voltage and current given in **Figure 17(a)** are maintained in phase.

In the time windows [0.3 to 0.8] and [1.5 to 2], where the PVG supplies the load by the maximum extracted power, the surplus of power is injected into the grid as noticed in **Figure 11.**

In the time between 0.8s and 1s is the load demanded a growing power demand is 12000w, and the PV power is lower than this load demand. Therefore, the grid recompenses this lack of power. In this case, the grid voltage and current are kept in phase opposition as shown in **Figure 17(b)** because the grid current reflects its direction. For the residual time span, the load demand takes the value of the maximum extracted power of the PV array and there is no power to be injected into the grid as shown in **Figure 11.**

Without overshoot following any change in sol irradiance or any variation of load power compared with PIC. The FLC provides a suitable non-linear control action compared to the linear PIC. Furthermore, the PIC parameters necessitate an accurate mathematical model of the system to be tuned, whereas the FLC technique does not require precise mathematical models for its designing and tuning, and it functions efficiently in case of imprecise, uncertain, and obscure models.

Also, the obtained simulation results were carried out that the 9LSCI can boost up the output voltage four times than the input voltage with high performance with fewer components as shown in **Figure 18** is the voltage of output 9LSCI is a waveform stairway shape with a maximum value of 400V= 4*Vin and an acceptable tolerable THD coefficient (16.43%) by using FL-RTO-SPWM technique.

According to **Table 5**, it is very better to use an FLC-RTO-PWM technique than others SPWM techniques. It is observed that THD performance with FLC-RTO-PWM is better than that of the other techniques.

Figure 19(a) displays the spectrum analysis of the current grid, which has a sinusoidal waveform with 0.28 % of THD in the case of using a classic PIC that is reduced to 0.23 % when applying FLC to control the current grid as shown in **Figure 19(b)** with using classical SPWM strategy.

Furthermore, the use of optimum values angles of switching strategy SPWM that is obtained by the RTO algorithm to control the switching of 9LSCI is a highly important criterion to minimize the total harmonic distortion, as FFT analysis of the grid, the current is presented in **Figure 19 (d)** shows the performance of the modulation strategy (i.e. RTO-SPWM) proposed to control 9LSCI proved that a quasi-sinusoidal current can be injected Into the grid with a total harmonic distortion rate of 0.19 % and 0.16 % for RTO-PWM is better than other SPWM techniques so it is very better to use an FLC-RTO-PWM technique in the grid-connected PV systems.

4. CONCLUSION

In this paper, a novel multicarrier SPWM technique to control the switching of a 9LSCI was proposed to inject PV power into the grid with minimum THD that is obtained by the RTO algorithm. This inverter can produce a high gain voltage that increases four times the output voltage by using low voltage input with the minimum number of

DOI: http://doi.org/10.17509/ijost.v7i1
p- ISSN 2528-1410 e- ISSN 2527-8045

components. The efficiency of the fuzzy logic controller is very satisfying with a reduced number of harmonic distortion, and it achieves high-quality outputs. It can attain an optimum THD value of 0.21 % when compared to the classic PIC. However, the addition of the RTO algorithm to search for the optimum initial angles of novel multi carriers SPWM technique to control the switching of 9LSCI has much better performance. An improvement of 0.12% in THD is observed compared with the classical multi carriers SPWM technique. It is not a secret that the proposed RTO-SPWM technique used to control the switching of 9LSCI resulted in an optimal combination between is the first, the minimizing of the number of switches and components when compared with the classical MLI, the second, the performance of the new modulation strategy RTO-SPWM proposed has a benefit of the photovoltaic power injected into the grid with THD value has been greatly reduced until it reaches 0.16 % thus the current becomes very close to sinusoidal current. Moreover, the RTO algorithm comes with better performance, in terms of accuracy and stability, and it functions competently with complex systems as the classical meta-heuristic optimizations techniques.

5. AUTHORS' NOTE

The authors declare that there is no conflict of interest regarding the publication of this article. The authors confirmed that the paper was free of plagiarism.

6. REFERENCES

Benamor, A., Benchouia, M., Srairi, K., and Benbouzid, M. (2019). A novel rooted tree optimization apply in the high order sliding mode control using super-twisting algorithm based on DTC scheme for DFIG. *International Journal of Electrical Power and Energy Systems, 108*, 293-302.

Gopal, Y., Panda, K. P., Birla, D., and Lalwani, M. (2019). Swarm optimization-based modified selective harmonic elimination PWM technique application in symmetrical H-bridge type multilevel inverters. *Engineering, Technology and Applied Science Research, 9*(1), 3836-3845.

Labbi, Y., Attous, D. B., Gabbar, H. A., Mahdad, B., and Zidan, A. (2016). A new rooted tree optimization algorithm for economic dispatch with valve-point effect. *International Journal of Electrical Power and Energy Systems, 79*, 298-311.

Maamir, M., Charrouf, O., Betka, A., Sellali, M., and Becherif, M. (2020). Neural network power management for hybrid electric elevator application. *Mathematics and Computers in Simulation, 167*, 155-175.

Mali, S., and Patil, B. (2018). THD minimization in multilevel inverter using optimization approach. *International Journal of Engineering Research and Technology (IJERT), 7*(6), 97-100.

Marmouh, S., Boutoubat, M., and Mokrani, L. (2018). Performance and power quality improvement based on DC-bus voltage regulation of a stand-alone hybrid energy system. *Electric Power Systems Research, 163*, 73-84.

DOI: http://doi.org/10.17509/ijost.v7i1
p- ISSN 2528-1410 e- ISSN 2527-8045

Meraj, M., Rahman, S., Iqbal, A., Ben-Brahim, L., and Abu-Rub, H. A. (2020). Novel level-shifted PWM technique for equal power sharing among quasi-z-source modules in cascaded multilevel inverter. *IEEE Transactions on Power Electronics, 36*(4), 4766-4777.

Nouaiti, A., Saad, A., Mesbahi, A., and Khafallah, M. (2017). Implementation of a single phase switched-capacitor nine-level inverter for PV system applications with selective harmonic elimination. *International Journal of Computer Applications, 168*(7), 9-15.

Nouaiti, A., Saad, A., Mesbahi, A., and Khafallah, M. (2018). Experimental implementation of a low-cost single phase five-level inverter for autonomous PV system applications without batteries. *Engineering, Technology and Applied Science Research, 8*(1), 2452-2458.

Qi, Q., Ghaderi, D., and Guerrero, J. M. (2021). Sliding mode controller-based switched-capacitor-based high DC gain and low voltage stress DC-DC boost converter for photovoltaic applications. *International Journal of Electrical Power and Energy Systems, 125*, 106496.

Sandeep, N., and Yaragatti, U. R. (2017). A switched-capacitor-based multilevel inverter topology with reduced components. *IEEE Transactions on Power Electronics, 33*(7), 5538-5542.

Sannigrahi, S., Ghatak, S. R., and Acharjee, P. (2019). Fuzzy logic–based rooted tree optimization algorithm for strategic incorporation of DG and DSTATCOM. *International Transactions on Electrical Energy Systems, 29*(8), e12031.

Sen, P., Bana, P. R., and Panda, K. P. (2019). Firefly assisted genetic algorithm for selective harmonic elimination in PV interfacing reduced switch multilevel inverter. *International Journal of Renewable Energy Research (IJRER), 9*(1), 32-43.

Singh, A. S. a. M. J. a. S. (2015). Analysis of THD and output voltage for seven level asymmetrical cascaded h-bridge multilevel inverter using LSCPWM technique. *nternational Journal of Computer Applications, 112*(1), 1-6.

Tariq, M., Meraj, M., Azeem, A., Maswood, A. I., Iqbal, A., and Chokkalingam, B. (2018). Evaluation of level-shifted and phase-shifted PWM schemes for seven level single-phase packed U cell inverter. *CPSS Transactions on Power Electronics and Applications, 3*(3), 232-242.

Teja, S. R., Sankar, P. U., and Rajkumar, Y. (2017). Switched capacitor seven-level inverter. *International Journal of Pure and Applied Mathematics, 114*(12), 535-543.

Tiar, M., Betka, A., Drid, S., Abdeddaim, S., Becherif, M., and Tabandjat, A. (2017). Optimal energy control of a PV-fuel cell hybrid system. *International Journal of Hydrogen Energy, 42*(2), 1456-1465.

Youssef, B., Ahmed, N., Sanaa, H., and Mohamed, H. (2019). Selective-harmonic elimination with an optimized multicarrier modulation techniques for cascaded h-bridge multilevel inverter. *Journal of Applied Mathematics and Computation (JAMC), 3*(1), 574-582.

DOI: http://doi.org/10.17509/ijost.v7i1
p- ISSN 2528-1410 e- ISSN 2527-8045